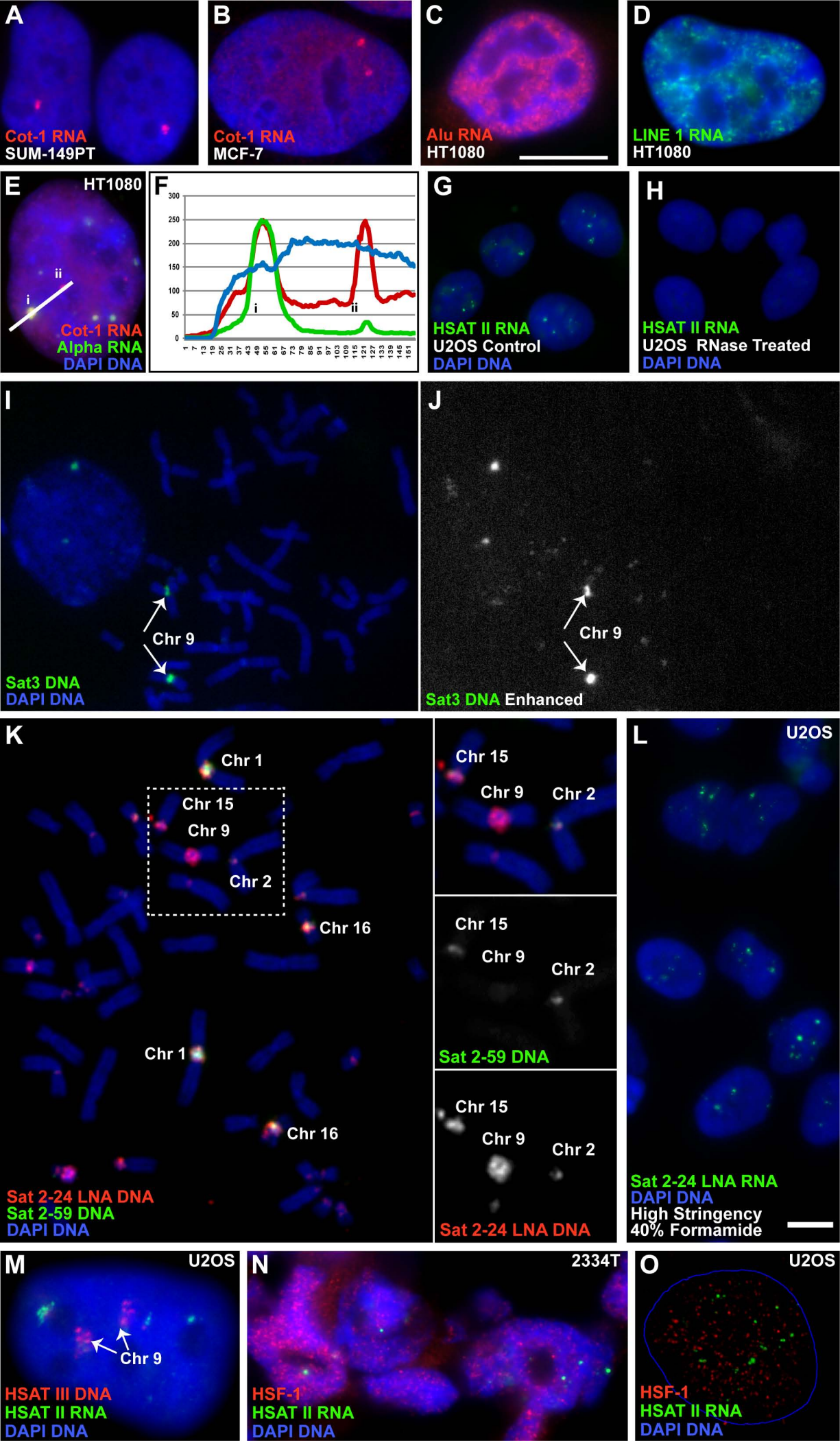
A
Cot-1 RNA
SUM-149PT
B
Cot-1 RNA
MCF-7
C
Alu RNA
HT1080
D
LINE 1 RNA
HT1080
E
HT1080
ii
i
Cot-1 RNA
Alpha RNA
DAPI DNA
F
300
250
200
150
100
50
0
i
ii
G
HSAT II RNA
U2OS Control
DAPI DNA
H
HSAT II RNA
U2OS RNase Treated
DAPI DNA
I
Chr 9
Sat3 DNA
DAPI DNA
J
Chr 9
Sat3 DNA Enhanced
K
Chr 1
Chr 15
Chr 9
Chr 2
Chr 16
Chr 1
Chr 16
Sat 2-24 LNA DNA
Sat 2-59 DNA
DAPI DNA
Chr 15
Chr 9
Chr 2
Chr 15
Chr 9
Chr 2
Sat 2-59 DNA
Chr 15
Chr 9
Chr 2
Sat 2-24 LNA DNA
L
U2OS
Sat 2-24 LNA RNA
DAPI DNA
High Stringency
40% Formamide
M
U2OS
Chr 9
HSAT III DNA
HSAT II RNA
DAPI DNA
N
2334T
HSF-1
HSAT II RNA
DAPI DNA
O
U2OS
HSF-1
HSAT II RNA
DAPI DNA

Fig S1. **CoT-1 and Satellite RNA foci in cancer cells, which are not associated with the HSATIII stress response (Related to Fig 1).** A-B) CoT-1 RNA signals show bright repeat RNA foci in breast cancer cell lines SUM-149 and MCF-7. C-D) Alu and L1 RNA do not accumulate into large RNA foci like CoT-1 RNA does. E-F) Some CoT-1 RNA foci in HT1080 cancer cells overlap with α-SAT RNA. White line in image is region measured in linescan. G-H) HSATII RNA foci are removed with RNAse treatment. I-J) The Sat3 probe on metaphase chromosomes predominantly labels the HSATIII locus on Chr 9. However, when the image is enhanced (J), very dim signals can be seen on HSATII loci on other chromosomes which may account for its ability to detect HSATII RNA. K) The Sat 2-24 LNA oligo under low stringency conditions (15% formamide) broadly detects HSAT II loci on about 10-12 different chromosomes, including the large HSATIII locus on Chr9 (see inserts at right), compared to the more restricted localization of the Sat2-59 probe. L) The Sat2-24 LNA probe still detects HSATII RNA foci well under high stringency hybridization conditions (40% formamaide). M) HSATII RNA is not emanating from the HSATIII locus on Chr9, labeled with the Sat3 probe under high stringency. N-O) Heat shock factor 1 (HSF-1) does not aggregate with HSATII RNA to form nuclear stress bodies (NSBs) in cancer nuclei *in vivo* (N) nor in the vast majority of cancer nuclei in culture (O). The blue DAPI DNA channel in (O) was replaced with the outline of the nucleus (blue) to better visualize the other signals.

Table S1: Satellite Expression in Cancer & Normal Cells/Tissue

Cancer Cell Line	Cell Type	Cot-1 RNA Foci	Aberrant HSATII RNA Foci	Aberrant α-Sat RNA Foci
HT-1080	Fibrosarcoma	+	+	+
MDA-MB-436	Breast Adenocarcinoma	+	No	+
U2OS	Osteosarcoma	+	+	No
SAOS-2	Osteosarcoma	+	+	
PC3	Prostate Adenocarcinoma	+	+	No
HEP-G2	Hepatocellular carcinoma	+	+	
MCF-7	Breast Adenocarcinoma	+	+	No
HCC-1937	Breast Ductal Carcinoma	+	+	No
T47D	Breast Ductal Carcinoma	+	+	
SUM-149pt	Inflammatory breast cancer	+		
HELA	Cervical Adenocarcinoma	+	No	No
MDA-MB-231	Breast Adenocarcinoma	No	No	No
JAR	Choriocarcinoma	No	No	No
HCT	Colon Adenocarcinoma		No	

Non-Cancer Cell Line	Cell Type	Cot-1 RNA Foci	Low level HSATII RNA	Low level α-Sat RNA
MCF-10A	Breast Fibrocystic Disease	No	No	+
IMR-90	Lung Fibroblast		No	
WS1	Embryonic Skin Fibroblast	No	No	+
TIG-1	Fetal Lung Fibroblast	No	No	+
Wi38	Fetal Lung Fibroblast	No		+
HFF	Foreskin Fibroblast	No	No	+
HSMM	Skeletal Myoblasts	No	No	+
HSMM	Differentiated Myotubes	No	No	+

Tissue Bank Identifier	Organ	Disease	Grade	Aberrant HSATII RNA Foci	Aberrant α-Sat RNA Foci
4386T	Breast	Adenocarcinoma	3	No	
2597T (-)	Breast	Carcinosarcoma	3	+/++	No
2389T	Breast	Ductal Carcinoma	1	No	No
0934T	Breast	Ductal Carcinoma IS	2	No	No
0934N	Breast	**Matched Normal**	n/a	No	No
1403T	Breast	Ductal Carcinoma	2	+++/+++	No
1533T	Breast	Ductal Carcinoma	2	No	No

2205T	Breast	Ductal Carcinoma	2	No	No
4596T	Breast	Ductal Carcinoma	2	No	
2334T	Breast	Ductal Carcinoma	3	+++/+++	++/+++
2334N	Breast	**Matched Normal**	n/a	No	No
2356T	Breast	Ductal Carcinoma	3	+/++	+/++
1659T	Breast	Ductal Carcinoma	3	+++/++	+/+
1659N	Breast	**Matched Normal**	n/a	No	
2175T	Breast	Lobular Carcinoma	3	No	No
2175N	Breast	**Matched Normal**	n/a	No	No
1645T	Breast	Lobular Carcinoma	n/a	No	No
1404T (-)	Breast	Lobular Carcinoma	2	No	No
4267T	Breast	Lobular Carcinoma	2	No	No
2004T	Breast	Metaplastic Carcinoma	2	++/++	No
2734T (-)	Breast	Metaplastic Carcinoma	3	++/+	++/++
0853T	Breast	Papillary Carcinoma	3	++/+	+/+++
0853N	Breast	**Matched Normal**	n/a	No	No
2243N	Breast	**Normal**	n/a	No	

Tissue Bank Identifier	**Organ**	**Disease**	**Grade**	**Aberrant HSATII RNA Foci**	**Aberrant α-Sat RNA Foci**
2081T	Ovary	Adenocarcinoma	3	++/++	No
2142M (+)	Ovary	Carcinoma (Metastatic)	3	++++/++	++/+++
2081N	Ovary	Not Malignant	n/a	No	No

Tissue Bank Identifier	**Organ**	**Disease**	**Grade**	**Aberrant HSATII RNA Foci**	**Aberrant α-Sat RNA Foci**
0575T	Brain	Astrocytoma	3	++/+++	++/++
1581T	Brain	Glioblastoma	4	+++/++++	No
1766T	Brain	Oligoastrocytoma	3	++/+	++/++
1796T	Brain	Medulloblastoma	4	+++/+	No
2980Ta	Brain	Glioblastoma	4	+/++++	No
4166T2	Brain	Glioblastoma	3	++/++	No
2373T	Colon	Adenocarcinoma	2	No	+++/+++
1880T	Kidney	Renal Cell Carcinoma	3	+/+	++/++
1880N	Kidney	**Matched Normal**	n/a	No	No
2311T	Lung	Squamous Cell Carcinoma	2	No	No
2312N	Pancreas	**Matched Normal**	n/a	No	
2312B	Pancreas	Serous Cystadenoma-Benign	n/a	No	No
0520T Lt	Prostate	Adenocarcinoma	7 (4+3)	No	No
0540T	Prostate	Adenocarcinoma	9 (4+5)	No	No
0827T	Prostate	Adenocarcinoma	7 (3+4)	No	No
1630T RT	Prostate	Adenocarcinoma	6 (3+3)	No	No
1673T	Stomach	Adenocarcinoma	2	No	
1673N	Stomach	**Matched Normal**	n/a	No	No
1689T	Stomach	GIST	3	+++/+	

2036T	Stomach	Adenocarcinoma	3	No	No
2210T	Stomach	Adenocarcinoma	3	++/++++	
2210N	Stomach	**Matched Normal**	n/a	No	No
2233T	Stomach	Adenocarcinoma	2	No	No
2036T	Stomach	Adenocarcinoma	3	No	No
2539T	Stomach	GIST	2	+++/+	No
2539N	Stomach	**Matched Normal**	n/a	No	No
2824T	Stomach	GIST	n/a	+/++	No
4136T	Stomach	Adenocarcinoma	3	++/++	No
2632T	Thyroid	Papillary Carcinoma	n/a	No	++/+
2632N	Thyroid	**Matched Normal**	n/a	No	No

Sample Number	**Sample Type**	**Diagnosis**	**Grade**	**Aberrant HSATII RNA Foci**	**Aberrant α-Sat RNA Foci**
1	Human Effusion	Poorly differentiated carcinoma of unknown primary	unknown	++	
2	Human Effusion	Breast lobular carcinoma	unknown	++	
3	Human Effusion	Pulmonary adenocarcinoma	3	+	
4	Human Effusion	Ovarian serous carcinoma	3	+	
5	Human Effusion	Renal clear cell carcinoma	unknown	+	
6	Human Effusion	Ovarian serous carcinoma	3	No	
7	Human Effusion	(Benign)	n/a	No	
8	Human Effusion	(Benign)	n/a	No	
9	Human Effusion	(Benign)	n/a	No	

Table S1. Aberrant HSATII RNA foci are present in most cancer cells and not normal cells (Related to Fig 1). Cancer and normal cell lines are listed first, followed by tissue samples then human effusion samples. The number of (+) on the left indicate the frequency of cells with CAST bodies in the sample and the (+) on the right indicates the frequency/size of CAST bodies per cell. n/a: Not applicable. Blank boxes indicate that sample was not examined for that property. Only large aberrant α-Sat RNA foci were scored as aberrant in cultured cancer nuclei, while small α-Sat RNA signals similar to those seen in normal cells were not. Due to poor RNA preservation in tissue samples no small α-Sat RNA foci were seen in normal tissue, so only large "aberrant" foci were seen or scored in cancer nuclei. Blue rows: tumor tissues that tested negative (-) for BRCA1 mutation status. Green rows: tumor tissues/lines that tested positive (+) for a BRCA1 mutation. Of the four negative effusion samples, three were from patients with no evidence of cancer on cytopathological analysis in clinical follow-up, whereas all other cases were from patients with malignant tumors. HSATII RNA foci were not seen in all cells in the effusion sample, but were restricted to cells primarily in clusters, showing nuclear enlargement and irregularity, consistent with malignancy.

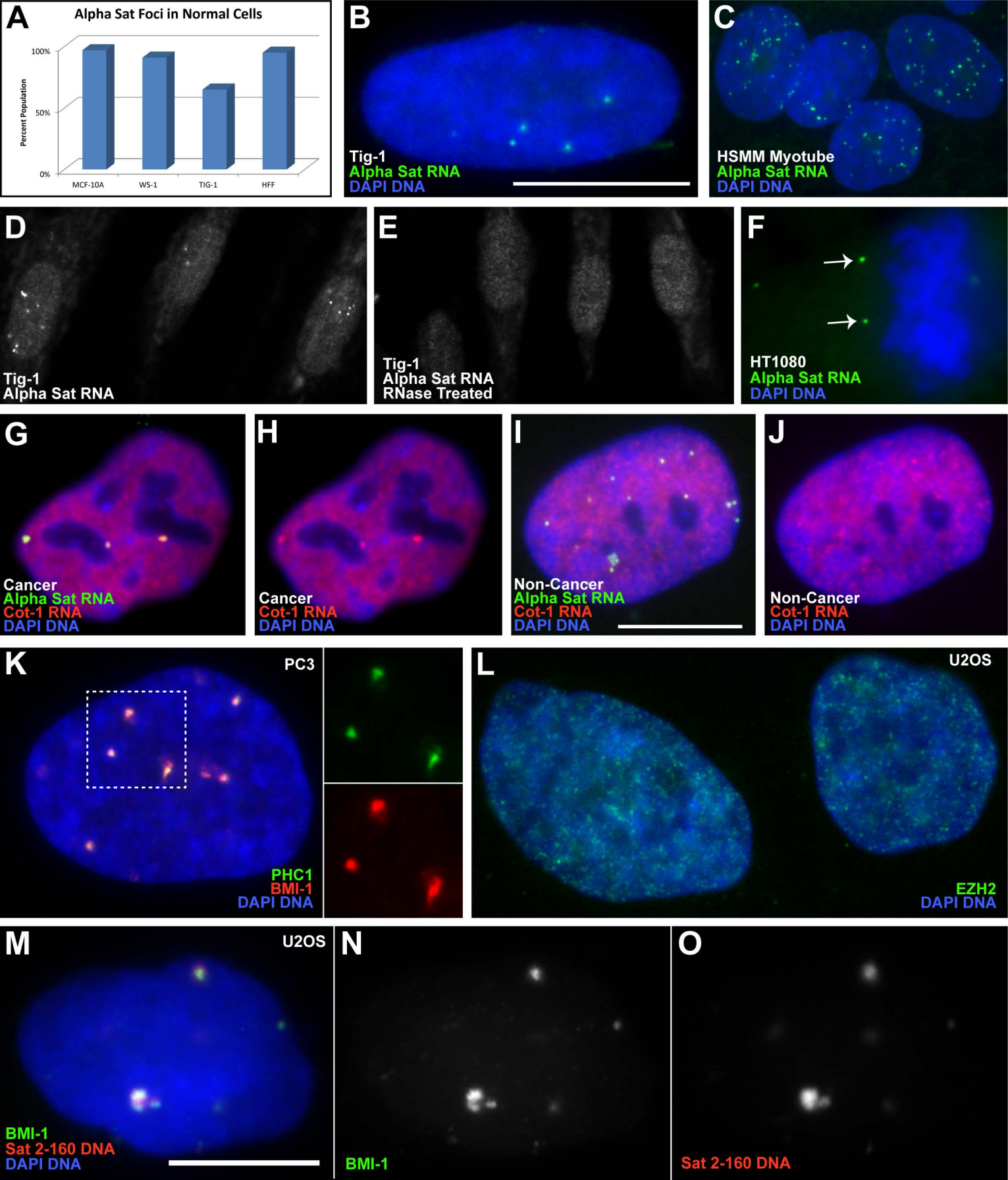
A
Alpha Sat Foci in Normal Cells
Percent Population
100%
50%
0%
MCF-10A
WS-1
TIG-1
HFF
B
Tig-1
Alpha Sat RNA
DAPI DNA
C
HSMM Myotube
Alpha Sat RNA
DAPI DNA
D
Tig-1
Alpha Sat RNA
E
Tig-1
Alpha Sat RNA
RNase Treated
F
HT1080
Alpha Sat RNA
DAPI DNA
G
Cancer
Alpha Sat RNA
Cot-1 RNA
DAPI DNA
H
Cancer
Cot-1 RNA
DAPI DNA
I
Non-Cancer
Alpha Sat RNA
Cot-1 RNA
DAPI DNA
J
Non-Cancer
Cot-1 RNA
DAPI DNA
K
PC3
PHC1
BMI-1
DAPI DNA
L
U2OS
EZH2
Cot-1 RNA
DAPI DNA
M
U2OS
BMI-1
Sat 2-160 DNA
DAPI DNA
N
BMI-1
O
Sat 2-160 DNA

Fig S2. Alpha-Sat RNA foci are seen in normal cultured cells, and other PRC1 proteins are found in cancer-associated BMI-1 bodies, but not usually PRC2 proteins (Related to Fig 1 & 2). A) Small α-Sat RNA foci were clearly and consistently visible, in all normal cell lines examined. 2-20 small RNA foci were readily apparent, without image processing in 65% to 97% of all normal cell populations. B-C) α-SAT RNA foci are easily visible by eye under the microscope in cycling fibroblasts (B) and non-cycling G0 differentiated myotube cells (C)(as well as the cycling myoblasts, not shown), but are significantly less robust than the satellite RNA foci in cancer cells. D-F) These α-Sat signals were confirmed as RNA by their removal by RNAse (E), and their release into the cytoplasm during mitosis (F: arrows). G-J) The aberrant α-Sat RNA foci seen in cancer cells differ from the normal α-Sat RNA foci by size and intensity which can be seen when looking at the Cot-1 RNA signal. The cancer-associated RNA foci (G) are so robust that they are responsible for the large Cot1- RNA foci visible over the nucleoplasmic Cot1 RNA signal (in separated image (H) at right), while α -SAT RNA foci in normal cells (I) are generally not abundant enough to produce CoT-1 RNA foci visible above the normal nucleoplasmic levels of CoT-1 RNA (J). K) PHC, a component of PRC1, is also found in CAP bodies with BMI-1 (inserts are separated channels of region). L) EZH2, components of PRC2, are not found in CAP bodies in most cancer lines (although one line, PC3, did have PRC2 in CAP bodies). M) The Sat2-160 probe (PCR generated from pUC1.77) is more restricted to 1q12, similar to the larger parent sequence pUC1.77 (see Fig 3A). These more restricted HSATII probes do not detect RNA foci well, but are highly correlated with CAP body formation (seen here with BMI-1 antibody).

Table S2: Presence of BMI-1 (CAP) Bodies in Cancer Tissue

Tissue Number	Organ	Disease	Grade	CAP Bodies
0575T	Brain	Astrocytoma	3	No
1581T	Brain	Glioblastoma	4	No
1766T	Brain	Oligoastrocytoma	3	No
1796T	Brain	Medulloblastoma	4	No
2980Ta	Brain	Glioblastoma	4	No
4166T	Brain	Glioblastoma	3	+
0853T	Breast	Papillary Carcinoma	3	+
0934T	Breast	Ductal Carcinoma IS	2	No
1403T	Breast	Ductal Carcinoma	2	No
1404T	Breast	Lobular Carcinoma	2	+
1553T	Breast	Ductal Carcinoma	2	No
1645T	Breast	Lobular Carcinoma		+
2004T	Breast	Metaplastic Carcinoma	2	+
2175T	Breast	Lobular Carcinoma	3	No
2334T	Breast	Ductal Carcinoma	3	+
2356T	Breast	Ductal Carcinoma	3	+
2389T	Breast	Ductal Carcinoma	1	No
2597T	Breast	Metaplastic Carcinoma	3	+
2597T2a	Breast	Metaplastic Carcinoma	3	+
2734T	Breast	Metaplastic Carcinoma	3	+
4267T	Breast	Lobular Carcinoma	2	No
4386T	Breast	Adenocarcinoma	3	No
4596T	Breast	Ductal Carcinoma	2	+
1880T	Kidney	Renal Cell Carcinoma	3	+
2081T	Ovary	Adenocarcinoma	3	+
2142M	Ovary	Carcinoma (Metastatic)	3	No
1689T	Stomach	GIST	3	No
2036T	Stomach	Adenocarcinoma	3	+
2210T	Stomach	Adenocarcinoma	3	No
2233T	Stomach	Adenocarcinoma	2	No
2539T	Stomach	GIST	2	No
2824T	Stomach	GIST		No
4136T	Stomach	Adenocarcinoma	3	+

Table S2: Large aggregates of BMI-1 are found in tumor nuclei *in vivo* (Related to Fig 2). Large BMI-1 aggregates are found in 44% of primary tumor samples (33 samples from 5 different organ systems). It is present is almost 60% of breast tumors tested.

Table S3: HSATII RNA Foci Size and Number in Cancer Cell Lines

Cell Line	Cell Type	Aberrant HSATII RNA Foci	# of aberrant Foci Average (Range)	Size of RNA Foci (microns) Average (Range)
U2OS	Osteosarcoma	+++	6 (3-11)	1.2 (0.9-1.6)
PC3	Prostate Adenocarcinoma	++	3 (1-6)	0.9 (0.8-1.0)
MCF-7	Breast Adenocarcinoma	++	2 (1-4)	0.98 (0.94-1.0)
T47D	Breast Ductal Carcinoma	+	2 (1-2)	0.35 (0.25-0.56)
SAOS-2	Osteosarcoma	+	1 (1-2)	0.2 (0.1-0.5)

Table S3. Number and size of aberrant HSATII RNA foci (Related to Fig 1 & 3). Most cancer cells contain only 1-3 HSATII RNA foci, suggesting very few loci are expressing. U2OS cells had the most HSATII RNA foci, which were not related to ploidy differences between lines. Datasheets supplied with the cell lines report chromosome numbers for T47D (~65), MCF-7 (~82), PC3 (~62) and U2OS (~70).

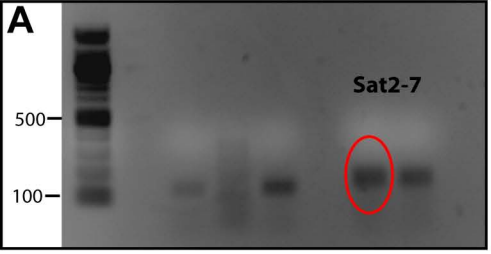

B

High SATII Expressors SRR182364 Database

hg18_chr1:147299811-147300507
hg18_chr1:147300535-147302452
hg18_chr10:38915450-38928835
hg18_chr10:41703232-41717296
hg18_chr10:41916703-41922088
hg18_chr10:41981563-41987614
hg18_chr16:33776379-33776829
hg18_chr16:33777847-33778427
hg18_chr16:33782203-33782656
hg18_chr16:33783449-33806096
hg18_chr16:34038041-34054531
hg18_chr16:44943305-45014085
hg18_chr16:45055159-45057995
hg18_chr17:22291242-22291353
hg18_chr2:90958833-90979427
hg18_chr2:91631250-91632651
hg18_chr2:91632685-91633785
hg18_chr2:91633804-91635721
hg18_chr2:91635733-91635968
hg18_chr2:91635996-91636334
hg18_chr22:15227855-15235597
hg18_chr22:15235651-15242475
hg18_chr7:57550259-57551005
hg18_chr7:57551906-57552150
hg18_chr7:57552619-57553068
hg18_chr7:57554068-57554465
hg18_chr7:57554596-57554880
hg18_chr7:57554903-57555110
hg18_chr7:57556155-57556938
hg18_chr7:57557778-57558628
hg18_chr7:57559489-57559654
hg18_chr7:61058277-61059078
hg18_chr7:61059094-61059232
hg18_chr7:61059252-61059534
hg18_chr7:61059562-61059829
hg18_chr7:61377290-61396834
hg18_chr7:61417257-61440549
hg18_chr7:64591285-64591659
hg18_chrY:12103443-12103612
hg18_chrY:12103642-12103905
hg18_chrY:12103979-12104337
hg18_chrY:12104361-12104618
hg18_chrY:12104644-12105562
hg18_chrY:12105589-12105809
hg18_chrY:12105836-12105998
hg18_chrY:27194329-27194390
hg18_chrY:27198241-27198303

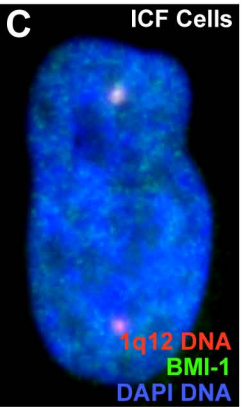

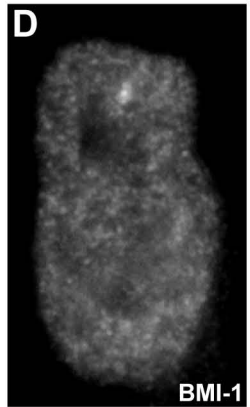

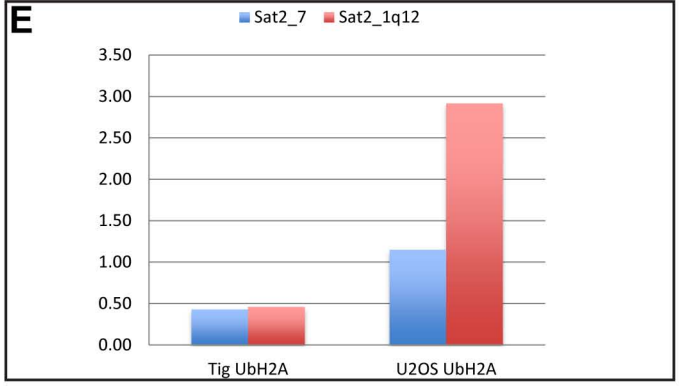

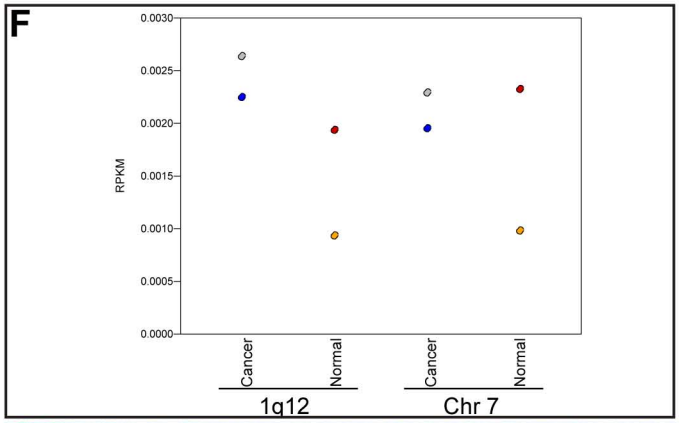

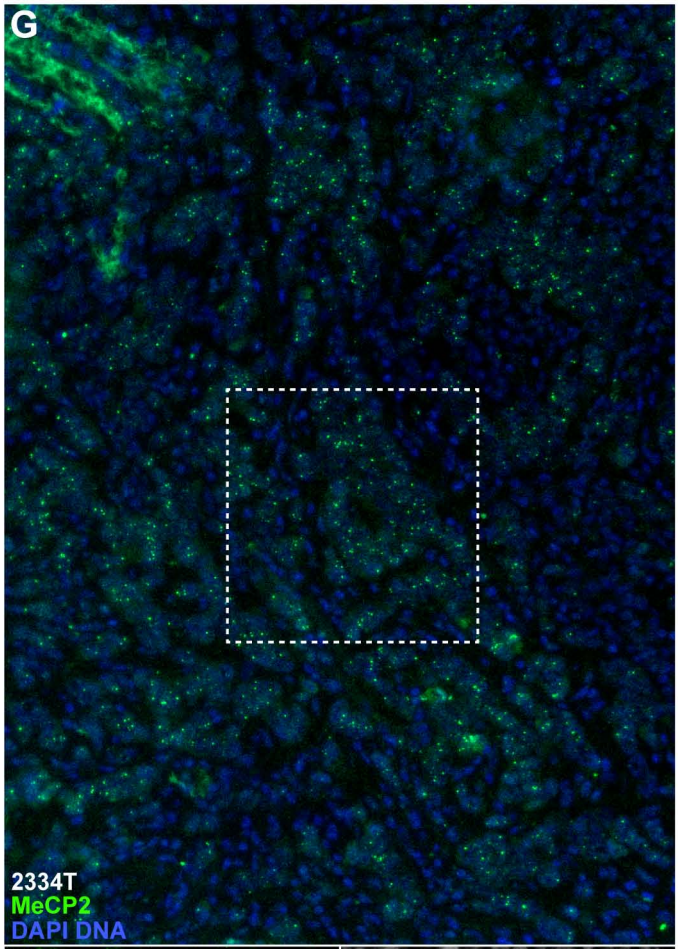

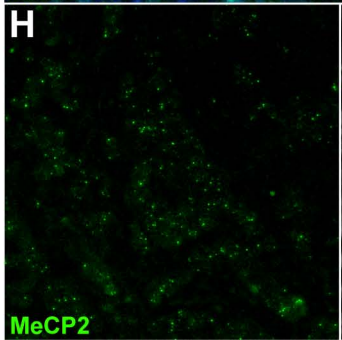

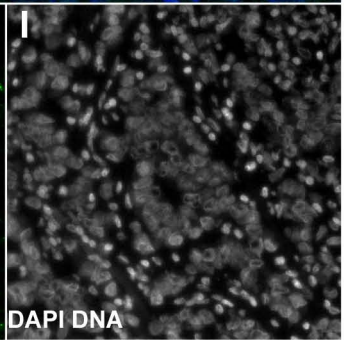

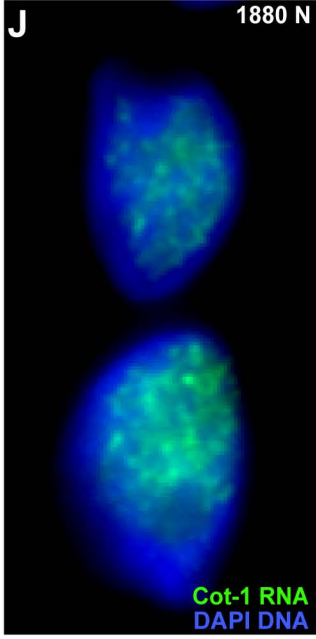

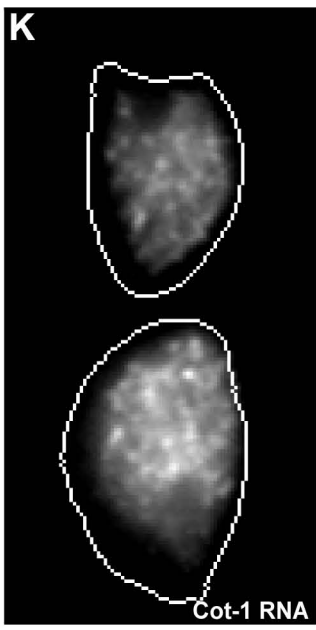

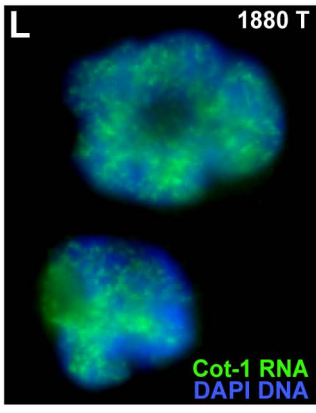

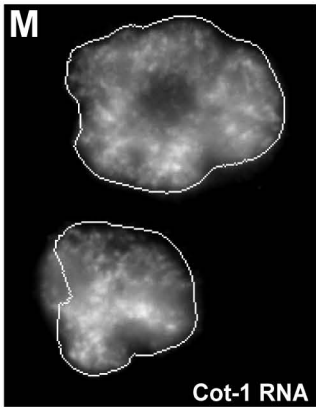

Fig S3. Locus specific CAP & CAST bodies may sequester factors and affect epigenetic regulation at other loci (Related to Fig 5 & 6). A) HSATII primer pairs amplify RNA in cancer cell lysates, with some exhibiting single prominent bands. Primers and RNA for the brightest band (Sat2-7) were used for further testing. B) A list of the highest HSATII expressers in the SRR182364 deep-seq pancreatic tumor database, mapped to the H19 human genome build. All sequences "mapping" to Chr7 are highlighted. C-D) CAP bodies (labeled with BMI-1) in human ICF cells are also localized to 1q12. Green channel separated in (D). E) ChIP-seq analysis reveals levels of UbH2A on 1q12 and Chr7 in normal (Tig-1) fibroblasts are similar, while in cancer nuclei (U2OS) UbH2A becomes enriched on 1q12 (Sat2-160) compared to Chr7 (Sat2-7). UbH2A on both Chr7 and 1q12 go up in cancer likely because many reads that "map" to Chr7 are also found on 1q12 (our Sat2-7 probe hybridizes well to 1q12 and 16q11 in situ), which is accumulating PRC1 and UbH2A. F) HSATII reads mapping to 1q12 are enriched in cancer (immortalized HMEL-BRAF (blue) & tumorigenic HMEL-BRAF (gray) cells) compared to normal cells (foreskin (red) & breast (orange) fibroblasts). G-I) MeCP2 "CAST" bodies are apparent even at low magnification (G). MeCP2 (H) and DNA (I) color channels are separated for indicated region in (G). J-K) CoT-1 repeat RNA is restricted to the euchromatic compartment in nuclei from a normal kidney tissue section, leaving a CoT-1 RNA free rim around the edge of the nucleus where the peripheral heterochromatic compartment (PHC) is located. Green channel with nuclear outline is separated at right (K). L-M) Heterochromatin is often lost in cancer nuclei, including the PHC, and can be seen in these tumor nuclei from kidney tissue sections where the CoT-1 RNA free region is less apparent. Green channel with nuclear outline is separated below (M).

Table S4: Ontology of affected genes in cancer cells

FuncAssociate Analysis for ubH2A ChiP-seq (Cancer vs Normal cells)

LOD	P	Adj. P	Attrib. ID	Attrib. name
1.0381252825	1.3 x 10-5	0.036	GO:0021953	central nervous system neuron differentiation
1.0155082058	1.9 x 10-5	0.044	GO:0000982	RNAPII core promoter proximal region sequence-specific DNA binding transcription factor activity
0.8454155349	2.4 x 10-6	0.004	GO:0000981	sequence-specific DNA binding RNAPII transcription factor activity
0.7804181465	5.4 x 10-7	0.001	GO:0030182	neuron differentiation
0.5679174144	6.6 x 10-10	<0.001	GO:0043565	sequence-specific DNA binding
0.5031703669	2.7 x 10-10	<0.001	GO:0003700	sequence-specific DNA binding transcription factor activity
0.50265432	2.8 x 10-10	<0.001	GO:0001071	nucleic acid binding transcription factor activity
0.441831619	2.2 x 10-6	0.004	GO:0048731	system development
0.4177001266	5.5 x 10-7	0.001	GO:0006357	regulation of transcription from RNAPII promoter
0.3027736649	1.8 x 10-5	0.042	GO:048869	cellular developmental process
0.2947269741	5.2 x 10-6	0.011	GO:0048856	anatomical structure development
0.2901777826	3.6 x 10-6	0.006	GO:0003677	DNA binding
0.2787754482	2.6 x 10-6	0.005	GO:0006355	regulation of transcription, DNA-dependent
0.2678311054	2.2 x 10-6	0.004	GO:0031326	regulation of cellular biosynthetic process
0.2632783511	3.2 x 10-6	0.006	GO:0009889	regulation of biosynthetic process
0.26305348	8.1 x 10-6	0.024	GO:0051252	regulation of RNA metabolic process
0.2593477784	8.0 x 10-6	0.023	GO:2000112	regulation of cellular macromolecule biosynthetic process
0.2549791855	6.5 x 10-6	0.021	GO:0019219	regulation of nucleobase, nucleoside, nucleotide and nucleic acid metabolic process
0.2491169125	9.4 x 10-6	0.024	GO:0051171	regulation of nitrogen compound metabolic process
0.2480638777	1.8 x 10-5	0.042	GO:0010556	regulation of macromolecule biosynthetic process
0.2290019303	1.6 x 10-5	0.039	GO:0031323	regulation of cellular metabolic process

Disease Ontology for RING1B/RNF2 ChiP-seq (Cancer vs Normal cells)

Binomial FDR	Disease Ontology term
2.0140×10^{-35}	physical disorder
3.0511×10^{-13}	congenital nervous system abnormality
6.9370×10^{-12}	hereditary breast ovarian cancer
2.5345×10^{-11}	aniridia
2.9984×10^{-11}	Rieger syndrome
4.0468×10^{-11}	nesidioblastosis
5.7277×10^{-3}	testicular neoplasm

Table S3: Genes that change the most for UbH2A or Ring1B in cancer cells are enriched for PcG regulated genes and with neoplastic association (Related to Fig 6). FuncAssociate analysis**:** UbH2A ChiP-seq data were used to select genes with the highest reduction (4-fold or greater) in UbH2A enrichment in U2OS versus Tig-1 cells. The selected genes were queried for Gene Ontology attributes using the web-based tool FuncAssociate. Gene Ontology terms with known associations to regulation by PcG proteins are highlighted in red. Disease Ontology: Selected significant Disease Ontology terms from gene ontology analysis of differential RING1B occupancy between normal fibroblast and melenoma cells are reported. The putative regulatory target genes underlying this table exhibited RING1B occupancy in normal fibroblast cells without any corresponding occupancy in tumor cells, based upon peak detection ($p < 10^{-5}$) using MACS. Differentially occupied RING1B ChIP-seq peaks were analyzed using GREAT (default gene association rule) with the Disease Ontology gene-sets.

SUPPLEMENTAL RESULTS

Satellite Probes and Hybridization Differences (Related to Figures 1 & 3):

Alpha-satellite (α-Sat) is comprised of a tandemly repeated 171 bp sequence at the centromere proper of all human chromosomes. The classical pericentric HSATII and HSATIII are comprised of highly repeated shorter sequences that share similarity. The tandemly repeated ~26bp HSATII consensus sequence (Jeanpierre, 1994) contains degenerate forms of the 5bp (ATTCC) HSATIII motif from Chr9 (Prosser et al., 1986). We used many different probes (see listed in Methods below) and hybridization conditions to allow us to discriminate satellite loci and RNA.

Non-LNA Probes: HSATII probes (Sat2-24nt, Sat2-59nt, Sat2-160bp, & puc 1.77kb) are distinct from one another (probes would not cross-hybridize), and appear to detect different "families" of HSATII (e.g. Fig S1K). Probes labeled loci with different intensity, likely proportional to the abundance of that sequence (and its level of conservation) at different loci. Sat2-160bp and puc 1.77kb are the most restricted to 1q12 and 16q11, and do not detect the small HSATII loci on other chromosomes well.

LNA probe: The degeneracy of many repeat sequences makes it difficult to design probes/primers that broadly detect all copies in the genome. The Sat2-24nt LNA probe detects HSATII the most broadly of all the probes used, at both low and high stringency. This is due to the unique biology of LNA oligos that allow hybridization with a high degree of mismatches due to the highly stable binding properties of the oligo. Hybridization to metaphase chromosomes with the Sat 2-24 LNA oligo detects the large HSATII loci on Chr 1 and 16 as well as small signals on a number of other chromosomes, consistent with a prior report (Eymery et al., 2010; Silahtaroglu et al., 2004). This probe, under low stringency (15% formamide) conditions, is also capable of detecting the more conserved HSATIII locus on Chr 9 (Fig S1K; see inserts at right).

RNA Detection: Generally, the probes that were restricted to 1q12 and 16q11 did not detect RNA foci, but localize with CAP bodies well. In the course of testing several HSATII probes that exhibited differences in RNA detection, we found that while all probes contained sequences that label Chr1 and 16 by DNA hybridization, only the probes that *also label the loci on the other chromosomes well* (including the Sat3 probe at low stringency; see below) detect RNA (since those are the loci expressing RNA).

HSATIII: Because HSATII sequences are degenerate versions of the more conserved 5bp HSATIII sequence and often contain these sequences, the Sat3 oligo (see probe list above), under low stringency, could detect the same HSATII RNA foci as the Sat 2-24 LNA oligo. Similarly, the permissive HSATII LNA probe also detects HSATIII sequences in DNA hybridization at low stringency (Fig S1K). On metaphase spreads, the Sat3 oligo was more specific detecting DNA than it was detecting RNA, and hybridized predominantly to the HSATIII locus on Chr 9 even under low stringency (Fig S1I-J). However, when the low stringency image is enhanced, very dim signals can be seen on HSATII loci on other chromosomes, again suggesting some cross hybridization to sequences in HSATII loci known to express, and explaining the cross hybridization to HSATII RNA foci. Under high stringency hybridization conditions (see below & Methods) the HSATIII probe is more restricted to the large Chr9 locus, which does not appear to be making RNA (Fig S1M). This confirms that the HSATIII oligo was detecting HSATII RNA under low stringency conditions and not HSATIII RNA associated with Chr 9 and nuclear stress bodies.

We used this HSATIII specific probe and high stringency conditions, as well as the heat shock factor 1 (HSF1) antibody, known to label HSATIII RNA in stress bodies (Fig S1N-O) (Biamonti and Vourc'h, 2010), to show that the unstressed cancer cells examined here were not producing HSATIII RNA, and that the HSATII RNA were not in nuclear stress bodies.

Identification of expressed locus on Chr7 (Related to Figure 3):

Most cancer nuclei have only 1-2 HSATII RNA foci (Table S3), suggesting very few loci express. Even in U2OS cells, with the highest number of HSATII RNA foci (which is not related to ploidy differences), most HSATII DNA

loci do not associate with an RNA focus (Fig 3E). To identify specific expressed sequences, we generated a set of 15 primer pairs designed using published 1q12 sequences and expressed sequences in RNA-seq data sets (Ting et al., 2011), to assay HSATII expression in cancer cells by RT-PCR. The majority of primer pair combinations produce the expected smear (or multiple bands) of HSATII from genomic DNA (consistent with divergent HSATII tandem repeats), however two pairs amplified distinct bands from RNA in U2OS cells and not in normal fibroblasts. When the RNA in these bands was sequenced, the sequences were more similar to one another (~90% identity) than the average identity of genomic HSATII sequences (~70%).

One primer pair (Sat 2-7) that amplified a very abundant RNA band in U2OS cells (Fig S3A), was used as a probe for RNA by FISH. It detected only 1-2 large HSATII RNA foci in U2OS (Fig 3F), which have numerous RNA foci (with the broader LNA probe), suggesting the Sat 2-7 probe detects RNA from a specific locus expressed in this osteosarcoma. It also labels the same 1-2 RNA foci in 3 of 5 tumor samples examined, that were detected with the permissive LNA probe, suggesting these tumors are only expressing RNA from this specific locus. Because most HSATII loci are not in the genome build, we could only tentatively map the expressed sequence to Chr7 (we got hits on Chr10 as well). We used commercially available centromere probes (Chr10, Chr2 and Chr7) to confirm expression was specific to Chromosome 7.

Sat2-7 sequence: TGGATCGAAACGAATCATCATTGAATGGAATCGAATGGAATCATCAT
CGAATGGAATCGAATGGAATGGACTCAAATGGAATGTGCTCGAATGGAATGGAATCGAAT
GGATTGATATCAAATAAAATGGAATGG

SUPPLMENTAL METHODS

Probes used:

Probe Name	Sequence	Label	Reference
Sat2-24nt LNA (Exiqon)	5'ATTCCATTCAGATTCCATTC GATC	5' Biotin	Exiqon, Product # 200501-03
Sat2-24nt (Invitrogen)	5'ATTCCATTCAGATTCCATTC GATC	5' Alexa 488	
Sat2-59nt Forward strand (Invitrogen)	5'ANTCCATTCGGGTCCATTC GATGATGATCACACTGGATT TCATTCCATAATTCT	3' Biotin or 5'FITC	(Prosser et al., 1986)
Sat2-59nt Reverse compliment (Invitrogen)	5'CGAATAGAATTATGGAATG AAATCCAGTGTGATCATCAT CGAATGGACCCGAATGGANT	5'FITC	
Sat2-160bp	Fwd primer: Sat2 PCR F 5'CATCGAATGGAAATGAAAG GAGTC Rev primer: Sat2 PCR R-inv 5'TTGACTGCAATCATCCAAT GGT	Biotin PCR label	(Alexiadis et al., 2007)
pUC1.77 (1q12)	1.77kb, Partial sequence in Cooke, 1979	Biotin or digoxigenin nick translation	(Cooke and Hindley, 1979)
Sat3 (Invitrogen)	5'CCATTCCATTCCATTCCATT	3'Biotin	(Prosser et al., 1986)
HuAlphaSat (59 mer)	CCT TTT GAT AGA GCA GTT TTG AAA CAC TCT TTT TGT AGA ATC TGC AAG TGG ATA TTT GG		Biosource & Invitrogen

HuAlu (33 mer)	CCC AAA GTG CTG GGA TTA CAG GCG TGA GCC ACC		Biosource
Sat2-1q12	Fwd primer: 5'GGAACCGAATGAATCCTCA TTGAATG Rev primer: ATGATTCCATTCGATTCAATG TTCCAT	Biotin PCR label	
Sat2-7	Fwd primer: 5' ATTCGATTCCATTCGATGATG ATTCC Rev primer: GGAACCGAATGAATCCTCAT TGAATG	Biotin or Dig PCR label or nick translation	

Human Cell Lines used:

1) HSMM: Skeletal Myoblasts (Cambrex)
2) SUM 149PT: Inflammatory Breast Cancer (Asterand)
3) TIG-1: Fetal Lung Fibroblast (Coriell)
4) RPE: Immortalized Retinal Pigment Epithelial (Gift from S. Temple NSCI)

5) HCC1937: Breast Ductal Carcinoma (ATCC)
6) HCT : Colon Adenocarcinoma (ATCC)
7) HeLa: Cervical Adenocarcinoma (ATCC)
8) Hep-G2: Hepatocellular carcinoma (ATCC)
9) HFF: Foreskin Fibroblast (ATCC)
10) HT1080: Fibrosarcoma (ATCC)
11) IMR-90: Lung Fibroblast (ATCC)
12) JAR: Choriocarcinoma (ATCC)
13) MCF7: Breast Adenocarcinoma (ATCC)
14) MCF-10A: Breast Fibrocystic Disease (ATCC)
15) MDA-MB-231: Breast Adenocarcinoma (ATCC)
16) MDA-MB-436: Breast Adenocarcinoma (ATCC)
17) PC3: Prostate Adenocarcinoma (ATCC)
18) hTERT RPE-1: Telomerase immortalized retinal epithelial (ATCC)
19) SAOS-2: Osteosarcoma (ATCC)
20) T-47D: Breast Ductal Carcinoma (ATCC)
21) U2OS: Osteosarcoma (ATCC)
22) Wi38: Fetal Lung Fibroblast (ATCC)
23) WS-1: Embryonic Skin Fibroblast (ATCC)
24) GM08747: ICF (immunodeficiency, centromeric heterochromatin instability, and facial anomalies) fibroblasts (Coriell)

Cell Fixation: Cultured cells were grown on glass coverslips prior to fixation. OCT frozen tissue blocks were cryosectioned onto cold glass slides (HistoBond+), and stored at -80 briefly until fixation. Human effusions were adhered to glass coverslips using CellTak (BD Biosciences) prior to fixation. Our standard fixation conditions used in most experiments has been previously published (Byron et al., 2013). Briefly, cells on glass coverslips are extracted in CSK buffer, 5% triton, and VRC (vanadyl ribonucleoside complex) for 1-3 min. Cells were fixed in 4% Paraformaldehyde for 10min, then stored in 1XPBS or 70% ETOH. Four fixations were tested on frozen tissue sections: 1) our standard fixation protocol summarized above (this produced the best results), 2) Fixed first, extracted second, and stored in ETOH. 3) Fixed (4% Paraformaldehyde) for 10min, no extraction, and stored in ETOH, and 4) 10min incubation in PreservCyt (Cytic Corp) at Rm temp and storage in ETOH.

RNA and DNA FISH & IF: Our standard hybridization conditions for RNA, DNA, simultaneous DNA/RNA , and simultaneous DNA/IF or RNA/IF detection was performed as previously described (Byron et al., 2013), and briefly

described below. All slides were counter stained with DAPI. Vectashield (Vector Labs) was used as mounting media for all fluorescence imaging.

Oligo hybridizations were done overnight at 37C, in 2xSSC, 1U/ul RNasin and 15% formamide, with 5pmol oligo or 0.1pmol LNA oligo as indicated for lower stringency, or at 40-50% formamide for higher stringency.

Larger probe hybridizations were overnight at 37C, in 2xSSC, 1U/ul RNasin and 50% formamide, with 2.5ug/ml of DNA probe. Cells were washed: 15% formamide/2xSSC at 37C (20min); 2xSSC at 37C (20min); 1xSSC at Rm temp (20min); and 4xSSC at Rm temp (5min).

Probe Labeling and detection: Larger (non-oligo) DNA probes were nick translated with biotin-11-dUTP or digoxigenin-16-dUTP (Roche Diagnostics, Indianapolis, IN). Oligos are ordered with biotin, dig or direct fluorochrome end labels (see table above). PCR generated probes incorporate fluorochrome conjugated nucleotides in the PCR reaction. Detection utilized Alexa 488 or Alexa 549 Streptavidin (Invitrogen) in 1%BSA/4xSSC for 1 hr at 37C. Postdetection washes: 4xSSC; 4xSSC with 0.1% Triton; and 4xSSC, each for 10 min at Rm temp, in the dark.

Simultaneous RNA/DNA hybridizations, RNA hybridization was performed before DNA denaturation and hybridization (as described above). Following RNA hybridization, the cells were fixed (4% Paraformaldehyde) for 10min, then treated with 0.2N NaOH in 70% ETOH for 5min, rinsed with 70% ETOH then denatured in 70% formamide, 2xSSC, at 75C for 2 min, before ethanol dehydration, and air-drying. Then DNA was hybridized and detected as described above.

Simultaneous RNA/ DNA and antibody detection: Most antibodies were used prior to RNA or DNA hybridization. Briefly, slides were incubated in the appropriate dilution of primary antibody in 1%BSA, 1xPBS and 1U/ul RNasin, for 1 hour at 37C. Slides were washed, and immunodetection was performed using 1:500 dilution of appropriately conjugated (Alexa 488 or Alexa 594, Invitrogen) secondary (anti-goat, mouse or rabbit) antibody, in 1xPBS with 1% BSA. The antibody signal is fixed in 4% paraformaldehyde for 10 min prior to hybridization (performed as detailed above).

Probes used: HSATII, HSATIII, α-SAT, & Alu sequences and info are listed above. 4kb human L1.3 ORF2 and 2kb human L1.3 ORF1 (from J. Moran, UMich), 10kb human XIST pG1A, human CoT-1 DNA (Roche), Centromere specific probes to Chr2, Chr10 & Chr7 (Aquarius Probes from Cytocell). RNA from various PCR experiments (Sat2-7, MeCP2 and Sin3A RIP) were cloned into a Strataclone vector (Agilent Cat no. 240205) prior to labeling for probes or for sequencing.

Antibodies used: BMI-1 (from Dr. David Weaver, Upstate & Abcam), Ring 1B, EZH2 and PHC-1 (Active Motif), MeCP2, EED and PTBP1 (PNC) (Abcam), and MBNL (from Dr. Charles Thorton), UbH2A (CellSignaling), H4K27me3 (Millipore).

NaOH & RNAse treatment: NaOH: Fixed cells were treated with 0.2N NaOH in 70% ETOH for 5min prior to RNA hybridization. RNase: Fixed cells were permeabilized with 0.1% triton-X in CSK buffer (4°C for 3min) then treated with 5μL/mL DNase-free RNase (Roche #11119915001) in PBS (3 hours, 37°C) prior to RNA hybridization.

5-AZA and EZH2 inhibition: Asynchronously growing cells on coverslips were treated with 5-aza-2'deoxycytidine (0.2ug/ml)(Sigma), and was added fresh to new media daily. 3-Deazaneplanocin A (DZNep) (5mM) (Cayman Chemical) was also added to some cultures to simultaneously inhibit EZH2.

ChIP-seq/ChIP-PCR: ChIP was performed as previously described (Yildirim et al., 2012) with some modification. Approximately $1x10^6$ cells were formaldehyde crosslinked to a final concentration of 1% for 10 minutes at room temperature and stopped with 125mM glycine. Cells were washed twice with 1xPBS containing protease inhibitors (Roche complete Mini protease inhibitor tablets) and pelleted at 100rpm at 4°C for 5 min. Cell pellets were resuspended in SDS lysis buffer (1%SDS, 10mM EDTA, 50mM Tris-Cl pH 8.1) with protease inhibitors and incubated on ice for 10 min. Cells were sonicated at 10% duty, setting 2 for 10 minutes to a fragment size of 150-500nt followed by centrifugation at 3000rpm for 10 min at 4°C. Supernatant was collected and 100uL chromatin was incubated with an antibody against Ubiquityl Histone H2A (UbH2A, Cell Signaling #8240) as per manufacturer's recommended concentrations at 4°C overnight with rotation in IP Buffer (.01% SDS, 1.1% Triton X-100, 1.2mM EDTA, 16.7mM Tris-Cl, pH 8.1, 167mM NaCl) + 0.5% BSA. 50uL protein G magnetic beads (Cell Signaling, #9006) was added to antibody-chromatin complex for 4 hours at 4°C with rotation. ChIP washes were as follows: 2X IP Buffer, 2X RIPA buffer (0.1% SDS, 10mM Tris, pH 7.6, 1mM EDTA, 0.1% Na-deoxycholate, 1% Triton X-100), 2X RIPA buffer + 0.3M NaCl., 1X LiCl Buffer (0.25M LiCl, 0.5% NP-40, 0.5% Na-deoxycholate), 1X TE. Crosslinks were reversed overnight at 65°C in 1X TE with the addition of 3% SDS, 1mg/mL proteinase K,

200mM NaCl. DNA was extracted with phenol:chloroform and precipitated with 0.1X volume 3M NaOAc, pH 5.2 and 2.5X volume 100% EtOH overnight at -20°C.

ChIP-Seq: Preparation of Illumina paired end deep sequencing ChIP libraries was performed as described (Yildirim et al., 2011). Deep sequencing data was mapped to human genome build hg19 using Bowtie (Langmead et al., 2009). Data normalization and peak calling was performed over a 10kb sliding window using SeqMonk (http://www.bioinformatics.babraham.ac.uk/projects/seqmonk/).

Ring1B ChIP-seq datasets: RNF2/Ring1B ChIP-seq datasets for normal fibroblasts (Pemberton et al., 2014)(raw data under GEO accession number GSE40740) and melanoma cells (Rai et al., 2015) (raw data under GEO accession number GSE51930) were analyzed. The quality of the ChIP-seq data was assessed using FastQC (S. Andrews (2010)) and reads were filtered for quality (i.e. Phred score) and the presence of (Illumina) primer sequences using Trimmomatic (Bolger et al., 2014) with the following single-end arguments: ILLUMINACLIP:TruSeq3- SE:2:30:10 LEADING:3 TRAILING:3 SLIDINGWINDOW:4:15 MINLEN:36. Reads were mapped to the human genome (hg19) using bowtie version 1.0.0 (Langmead et al., 2009) allowing up to 2 mismatches. Peaks were called using MACS version 2.1.1.20160226 (Zhang et al., 2008). ChIP-seq peaks with a p-value smaller than 10^{-5} were retained for subsequent comparison among tissues. In order to compare enrichment of RNF2/Ring1B at specific repetitive sequences, custom genomes were built and short reads were mapped using bowtie. In order to assess the genome-wide regulatory impact that loss of PRC1 availability between normal and cancer cells might imply, we compared localization of RNF2/Ring1B in fibroblasts (breast and foreskin) with that in melanoma cells (immortalized HMEL-$BRAF^{V600E}$ melanocytes and tumor cells derived from them) using the Disease Ontology terms in GREAT (McLean et al., 2010). RNF2/Ring1B loci ($p < 10^{-5}$) were used as input for gene-set testing with GREAT if they were present in both normal tissues and neither cancer tissue (Table S4B). Repeating the test with RNF2/Ring1B loci that are present in both cancer tissues and neither normal tissue, we detected two cancer-related terms: "neoplasm in vascular tissue" (binomial FDR < 1.8×10^{-7}) and "acoustic neuroma" (FDR < 3×10^{-5}).

RNA-IP (RIP): RIPs were carried out essentially as described (Jones et al., 1998; Long et al., 2011). U2OS cells ($1x10^8$) were suspended in cross-linking buffer (1X PBS supplemented with: 10 mM NaCl, 5 mM HEPES pH 7.%, 0.1 mM EDTA, 0.05 mM EGTA, 1% formaldehyde) for 30 min at Rm temp with rocking. The reaction was quenched with 50 mM glycine (pH 7.0) for 5 min at Rm temp then washed with 1X PBS and pelleted. Cells were lysed in 50 mM HEPES-KOH (pH 7.5), 140 mM NaCl, 1 mM EDTA, 1% Triton X-100, 0.1% sodium deoxycholate, protease inhibitors + RNase inhibitor (50 U/500 µl) and sonicated. $MgCl_2$ (25 mM), $CaCl_2$ (5 mM), RNase-free DNase I (100 U/500µl), and RNase inhibitor (3 µl/500 µl) were added and incubated at 37°C for 30 min. The reactions were centrifuged at 20,000 x *g* for 15 min at 4°C, keeping the supernatant for IPs. Cleared extract (100 µl) was diluted with 900 µl ChIP buffer (50 mM HEPES pH 7.5, 140 mM NaCl, 1 mM EDTA, 10% glycerol, and 0.5% NP-40) to which 5 ul antibody [MeCP2 7-18(Long et al., 2010), Sin3A(Jones et al., 1998), MBNL1 (M3320, Sigma), or normal rabbit serum (Sigma)] and 5 ul RNase inhibitor were added then rotated for 12 hrs at 4°C. Protein A/G Dynabeads (40 ul /RIP) were added to the RIP reactions for 1 hr, washed 3X in wash buffer (50 mM Tris pH 7.4, 500 mM NaCl, 1% Triton X-100, 0.1% SDS) and RNA was eluted in 200 µl Elution Buffer (200 mM NaCl, 50 mM Tris pH 7.4, 20 ug Proteinase K) for 1 hr at 42°C. Cross-linking was reversed by heating at 65°C for 5 hrs, and the RNA was extracted with acid equilibrated (pH 4.8) phenol:chloroform (5:1), ethanol precipitated with glycogen, and brought up in DEPC-dH_2O. RNAs were digested again with RNase-free DNase I for 20 min at 37°C, extracted and precipitated as above and brought up in 50 µl DEPC-dH_2O for use in RT-PCR (Sat II primers #). RT-PCR was performed on 5 µl RNA using the SuperScript III One-step RT-PCR system (Invitrogen) with the following cycling parameters: 94°C, 30 sec; 59°C, 15 sec; 68°C, 25 sec for 35 cycles. To control for DNA contamination, RNaseA (10 µg) was added to 5 µl RNA, incubated for 5 min and RT-PCR was performed in parallel.

Microscopy and Digital Imaging: Digital imaging was performed using an Axiovert 200 or an Axiophot Zeiss microscope equipped with a 100X PlanApo objective (NA 1.4) and Chroma 83000 multi-bandpass dichroic and emission filter sets (Brattleboro, VT), set up in a wheel to prevent optical shift. Images were captured with the Zeiss AxioVision software, and an Orca-ER camera (Hamamatsu, NJ). Where required, care was taken to eliminate any bleed-thru of Red fluorescence into the fluorescein channel. Most experiments were carried out a minimum of 3 times, and scored by at least two independent investigators. All findings were easily visible by eye through the microscope (unless otherwise noted), and images were minimally enhanced for brightness and contrast in Photoshop for publication (unless otherwise noted).

Digital quantification: All images compared or quantified for signal intensity were taken with the same exposure on the same day with the same microscope and fluorochrome.

Linescans: The Linescan function in the Metamorph Image analysis software (Molecular Devices, Inc.) was used to measure relative signal intensities for each channel of a 3 color digital image of cell nuclei. Line regions were drawn across the entire nucleus of individual cells (unless otherwise noted) and pixel intensity along the line measured. Y-axis is intensity of each pixel across the length of the line (X-axis).

Maximum pixel intensity vs. threshold: Metamorph software was used to measure the single maximum pixel intensity of each cell nucleus. Three color images were used and the color channels separated. The regions outlining the nuclei on the DNA color channel were transferred to the channel containing the RNA signals. The single brightest pixel in each nuclear region was measured. This was then plotted against a threshold calculated for each cell line using 3X the average lowest intensity pixel in each nucleus for that cell line.

Total Sat RNA signal/cell: Metamorph software was used, and color channels separated for 3 color images. Computer generated regions were drawn around all RNA signals in each nucleus. The average pixel intensity for each region was multiplied by the area of each region, and then all regions in each nucleus were added to give the integrated intensity (area and brightness) for each nucleus.

REFERENCES

Alexiadis, V., Ballestas, M.E., Sanchez, C., Winokur, S., Vedanarayanan, V., Warren, M., and Ehrlich, M. (2007). RNAPol-ChIP analysis of transcription from FSHD-linked tandem repeats and satellite DNA. Biochim Biophys Acta *1769*, 29-40.

Biamonti, G., and Vourc'h, C. (2010). Nuclear stress bodies. Cold Spring Harb Perspect Biol *2*, a000695.

Bolger, A.M., Lohse, M., and Usadel, B. (2014). Trimmomatic: a flexible trimmer for Illumina sequence data. Bioinformatics *30*, 2114-2120.

Byron, M., Hall, L.L., and Lawrence, J.B. (2013). A multifaceted FISH approach to study endogenous RNAs and DNAs in native nuclear and cell structures. Curr Protoc Hum Genet *Chapter 4*, Unit 4 15.

Cooke, H.J., and Hindley, J. (1979). Cloning of human satellite III DNA: different components are on different chromosomes. Nucleic Acids Res *6*, 3177-3197.

Eymery, A., Souchier, C., Vourc'h, C., and Jolly, C. (2010). Heat shock factor 1 binds to and transcribes satellite II and III sequences at several pericentromeric regions in heat-shocked cells. Exp Cell Res *316*, 1845-1855.

Jeanpierre, M. (1994). Human satellites 2 and 3. Ann Genet *37*, 163-171.

Jones, P.L., Veenstra, G.J., Wade, P.A., Vermaak, D., Kass, S.U., Landsberger, N., Strouboulis, J., and Wolffe, A.P. (1998). Methylated DNA and MeCP2 recruit histone deacetylase to repress transcription. Nat Genet *19*, 187-191.

Langmead, B., Trapnell, C., Pop, M., and Salzberg, S.L. (2009). Ultrafast and memory-efficient alignment of short DNA sequences to the human genome. Genome Biol *10*, R25.

Long, S.W., Ooi, J.Y., Yau, P.M., and Jones, P.L. (2010). A brain-derived mecp2 complex supports a role for MeCP2 in RNA processing. Biosci Rep *31*, 333-343.

Long, S.W., Ooi, J.Y., Yau, P.M., and Jones, P.L. (2011). A brain-derived MeCP2 complex supports a role for MeCP2 in RNA processing. Biosci Rep *31*, 333-343.

McLean, C.Y., Bristor, D., Hiller, M., Clarke, S.L., Schaar, B.T., Lowe, C.B., Wenger, A.M., and Bejerano, G. (2010). GREAT improves functional interpretation of cis-regulatory regions. Nat Biotechnol *28*, 495-501.

Pemberton, H., Anderton, E., Patel, H., Brookes, S., Chandler, H., Palermo, R., Stock, J., Rodriguez-Niedenfuhr, M., Racek, T., de Breed, L.*, et al.* (2014). Genome-wide co-localization of Polycomb orthologs and their effects on gene expression in human fibroblasts. Genome Biol *15*, R23.

Prosser, J., Frommer, M., Paul, C., and Vincent, P.C. (1986). Sequence relationships of three human satellite DNAs. J Mol Biol *187*, 145-155.

Rai, K., Akdemir, K.C., Kwong, L.N., Fiziev, P., Wu, C.J., Keung, E.Z., Sharma, S., Samant, N.S., Williams, M., Axelrad, J.B.*, et al.* (2015). Dual Roles of RNF2 in Melanoma Progression. Cancer Discov *5*, 1314-1327.
Silahtaroglu, A., Pfundheller, H., Koshkin, A., Tommerup, N., and Kauppinen, S. (2004). LNA-modified oligonucleotides are highly efficient as FISH probes. Cytogenet Genome Res *107*, 32-37.
Ting, D.T., Lipson, D., Paul, S., Brannigan, B.W., Akhavanfard, S., Coffman, E.J., Contino, G., Deshpande, V., Iafrate, A.J., Letovsky, S.*, et al.* (2011). Aberrant overexpression of satellite repeats in pancreatic and other epithelial cancers. Science *331*, 593-596.
Yildirim, E., Sadreyev, R.I., Pinter, S.F., and Lee, J.T. (2012). X-chromosome hyperactivation in mammals via nonlinear relationships between chromatin states and transcription. Nat Struct Mol Biol *19*, 56-61.
Zhang, Y., Liu, T., Meyer, C.A., Eeckhoute, J., Johnson, D.S., Bernstein, B.E., Nusbaum, C., Myers, R.M., Brown, M., Li, W.*, et al.* (2008). Model-based analysis of ChIP-Seq (MACS). Genome Biol *9*, R137.